SCIEPublish

Article

Efficacy and Cytocompatibility of a Pressure Garment—Silicone Composite Dressing Material for Scar Healing

Kam-Che Lui [1], Xungai Wang [1,2,*] and Chi-wai Kan [1]

[1] School of Fashion and Textiles, The Hong Kong Polytechnic University, Hung Hom, Kowloon, Hong Kong, China; kalina.kc.lui@connect.polyu.hk (K.-C.L.); kan.chi.wai@polyu.edu.hk (C.-w.K.)

[2] The Hong Kong Polytechnic University, Research Centre of Textiles for Future Fashion and Research Institute for Sports Science and Technology, Hung Hom, Kowloon, Hong Kong, China

* Corresponding author. E-mail: xungai.wang@polyu.edu.hk (X.W.)

Received: 27 February 2024; Accepted:13 May 2024; Available online: 28 May 2024

ABSTRACT: Pressure garment therapy (PGT) and silicone gel sheeting (SGS) predominate non-invasive interventions for burn injuries, but the market lacks a composite solution combining pressure garment fabric (PGF) and medical-grade silicone (e.g. Biopor®AB) for multi-therapeutic efficacy. To address this gap, a versatile composite dressing of PGF-Biopor®AB was developed. PGF-Biopor®AB incorporates dual PGF-SGS therapy, mechanotherapy, and active moisture management, to facilitate recovery of hypertrophic subsidiary structures. The PGF structure enables the application of PGT, while the Biopor®AB silicone characteristics enforce silicone gel therapy (SGT). The PGF-SGS efficacy optimization not only reduces tension but also facilitates water vapor and oxygen penetration, along with hydration of the stratum corneum. Mechanotherapy, involving tension-shielding and pressure redistribution, promotes the reorganization of the collagen-fiber network. For active moisture management, the incorporation of a microchannel structure with active nylon absorbency facilitates effective moisture control through water absorption, retention, and cellular pathways of transport. In this study, the microscale features in the structure were further investigated. Under ISO 10993-5 standard, an over 70% cell viability in 3-(4,5-dimethylthiazol-2-yl)-2,5-diphenyltetrazolium bromide (MTT) assay containing the L929 cell line verified the enhanced cell growth and inhibited proliferation, endorsing the safe usage of PGF-Biopor®AB. Patient studies of one-month efficacy in both high and low-cell-density samples and an early scarless healed wound suggest that over 70% cell viability is sufficient for optimal scar therapeutics. The multifaceted scar repair roles are fulfilled by addressing persistent inflammation, insufficient oxygenation, low levels of perfusion, and scar-healing tension, hence realising the multi-therapeutic efficacy of the composite dressing.

Keywords: Pressure garment, Silicone, Composite dressing, Dual therapy, Scar-healing

1. Introduction

The cell-surface structure is composed of a bimolecular lipid layer exhibiting viscoelastic properties, which manifest as non-Newtonian flow at high surface pressure [1]. As the cell surface experiences shear during movement, an increase in surface viscosity leads to reduced surface area and adhesiveness, a phenomenon termed “contact inhibition” [1]. In the context of scar healing, the literature indicates that fibroblasts on anisotropic structured patches exhibit altered cell growth and reduced proliferation, reflecting potential values of scar inhibition [2]. The microchannels in PGF-Biopor®AB, moulding from the printing screen mark, build a similar anisotropic structure, while the microscale surface characteristics may impact cell-surface interactions, assisting early-scarless wound healing and scar inhibition [3,4]. Specifically, the Biopor®AB viscoelastic characteristics and microscale topographic features favour cellular movements for high cell biocompatibility. Cell viability (%) is related to surface viscoelastic properties, roughness, and rigidity, providing vital information on fibroblast cell growth rates, and serving as a reference for cytocompatibility and scar-healing efficacy.

Cell viability (%), a quantitative count of healthy cells within PGF-Biopor®AB, is used to indicate the growth and lysis of cells, allowing the monitoring of cell behavior in the PGF-Biopor®AB scar-healing microenvironment. The

https://doi.org/10.35534/amsm.2024.10005

L929 mouse lung fibroblast cells can mimic physiological skin tissue scenarios during cell culture and have been used to evaluate cytocompatibility. MTT (3-(4,5-dimethylthiazol-2-yl)-2,5-diphenyltetrazolium bromide) is employed in the cell viability testing. Active cells metabolically reduce the yellow-colored tetrazolium MTT into an intracellular purple formazan through dehydrogenase enzyme activity [5–7]. The rate of tetrazolium reduction inversely corresponds to the rate of cell proliferation. Cellular toxicity is assessed by quantifying the purple formazan using a spectrophotometric method [5–7]. Cell viability exceeding 70% indicates good biocompatibility and the absence of cytotoxicity, indicating the clinical application potential of scar-healing dressing [8,9].

In this study, L929 cell lines were indirectly cultured on the micro-featured structure of PGF-Biopor®AB for 1 day and 3 days. The growth rate, as determined by cell viability (%), provides insights into cellular behavior in alignment, movement, adhesion, and proliferation. This relative cell viability ranking by different samples enables projections of scar-healing performance [10–12]. Beyond cytotoxicity assessment, PGF-Biopor®AB samples with high and low cell density (and >70% viability) were selected for scar-healing efficacy assessment in a one-month trial patient study and a non-healed wound, respectively. The Vancouver Scar Scale parameters were utilized to assess scar-healing efficacy in patients with degree-2 and degree-3 scarring skin and a non-healed wound. By comparing patient outcomes against literature records of PGT and silicone gel therapy (SGT) efficacies, improvements in scar-healing efficacy can be evaluated while concurrently assessing the scar therapeutics associated with >70% cell viability. This facilitates the establishment of a PDMS composite guideline for surface characteristics based on cell viability.

2. Experimental

2.1. Materials

The medical-grade silicone Biopor®AB (Dreve Otoplastik GmbH, Unna, Germany) was purchased from Widex Hong Kong Hearing & Speech Centre Ltd (PDMS in a room temperature vulcanization two-part formulation (RTV2)). Silicone gel sheeting (SGS, Cica-Care®, Smith and Nephew, England) was officially supplied for control. Screens with a mesh size of #1000 (i.e., 1000 openings per square inch) and #2000 in wooden frames of 8″ × 10″ and 14″ × 20″ were used. Tony Screen of Jet T Technology from C1A. G/F, 72 Hoi Yuen Rd, Kowloon, supplied the screens. Aveeno® skin relief moisturising lotion was ordered from Market Place supermarkets. Pressure garment fabric (PGF) is a public hospital occupation-use material and was sourced from Polliam Trading Corp. Ltd. (Hong Kong, China). Cell culture components including L-Glutamine solution, Penicillin-Streptomycin solution, alpha modification of minimum essential medium (αMEM) and 0.25% Trypsin solution were purchased from Hy Clone. Phosphate buffer solution (PBS) was purchased from Uni Region Biotech. 3-[4,5-Dimethylothiazol-2-yl]-2,5 diphenyl tetrazolium bromide (MTT) and Dimethyl sulfoxide (DMSO) were purchased from SIGMA Chemical Limited; horse serum was purchased from GIBCO™ of Thermo Fisher Scientific, and high-density polyethene (HDPE) and Zinc Di-ethyldithio-carbamate (ZDEC) were purchased from Food and Drug Safety Center (FDSC).

2.2. Fabrication of PGF-Biopor®AB

The screen printing of the scar healing composite (PGF-Biopor®ABs) was conducted using raw materials from Biopor®AB and PGF; the process flow is depicted in Figure 1. The same fabrication method as previously reported was adopted [13]. To assess the impact of screen size, two screens (#1000 and #2000) were utilized. The PGF-Biopor®AB samples were single-layer screen printed on PGF, and they were labelled as PGF-x-y, where x indicated the screen number and y indicated the number of printing layers. All prepared samples, along with controls (Cica-care® and PGF), were stored under standard conditions at 65 ± 2% relative humidity and 20 ± 2 °C for a minimum of 24 h before subsequent measurement and testing [14–17].

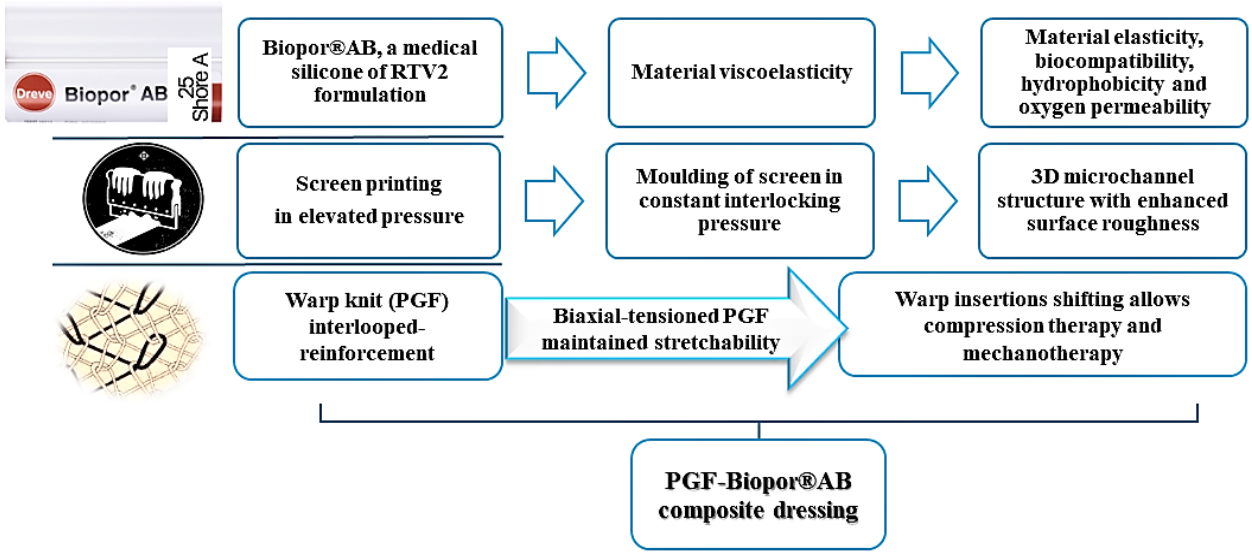

Figure 1. Process flow diagram for fabrication of PGF-Biopor®AB Composite.

2.3. Surface and Structural Features Characterization

A Leica digital microscope (M165C with HD290, Leica Mikrosysteme Vertriebs GmbH, Wetzlar, Germany) was utilized for the inspection of surface morphologies. To enhance structural contrast in optical microscopy (OM) sample preparation, staining with Dispersol blue D-2R (3%) was applied. For a comprehensive examination of surface and interfacial morphologies, an electronic scanning microscope (SEM) (Hitachi TM3000, Angstrom Scientific, New Jersey, USA) was employed.

2.4. Cytotoxicity Testing and Trial Patient Study

2.4.1. Cell Proliferation Assay

The cytotoxicity of PGF-Biopor®AB was evaluated using the mouse lung fibroblast L929 cell line where L929 cells mimicked the physiological scenarios of the skin tissue. Figure 2 lists the flowchart of the MTT test in ISO-10993-5 standard. For cell culture, fibroblast L929 cells were first incubated in αMEM medium with 10% horse serum at 37 ± 1 °C in the presence of 5 ± 1% CO_2, which were then used as extraction buffer for a dilution series of different extracts (100%, 50%, 25%, 12.5%) under 37 ± 1 °C for 24 ± 2 h with constant agitation at 100 rpm. Three Controls were also prepared for comparative study and quality criteria as below:

Blank control: αMEM medium with 10% horse serum.

Positive control: Polyurethane film—Polyurethane film containing Zinc Di-Ethyldithio-carbamate (ZDEC), (RM-A, Hatano research institute, Japan), extracted with 0.1 g ± 10%/1 mL αMEM.

Negative control: high density poly-ethylene (HDPE) film, (RM-C, Hatano research institute, Japan).

All extracts and controls were put into the 96-well plate and then incubated at 37 ± 1 °C in the presence of 5 ± 1% CO_2 for the requested time (24 h for a 1-day test, 72 h for a 3-day test). Results were collected at the end of individual tests; the inhibition of cell viability of positive control was greater than 30% and negative control was less than 30%.

1. Inhibition of cells in α MEM medium with 10% horse serum

2. 37 ± 1 °C in the presence of 5 ± 1% CO_2 for 24 ± 2 h

3. Extracts (100%, 50%, 25%, 12.5%) & controls (blank, positive, negative)

4. 37 ± 1 °C in the presence of 5±1% CO_2 for 24 ± 2 h

5. Morphology investigation

6. Adding DASO

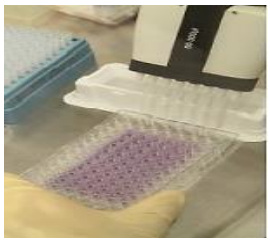

7. Adding MTT

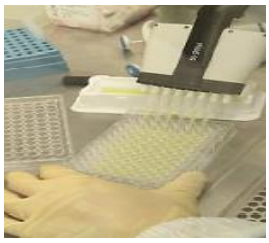

8. Data collection

Figure 2. Flowchart of MTT essay test in ISO-10993-5 standard.

2.4.2. Cell Viability Assay

The cytocompatibility of both PGF-Biopor®AB and control (Cica-care©) was examined by assessing the viability of L929 cells using the MTT assay. The selected samples for this assessment were PGF-1000-6, PGF-2000-6, PGF-1000-50, and PGF-2000-50 (see section 2.2 for sample labelling protocol). To facilitate subsequent discussion and analysis, physical data of various PGF-Biopor®ABs and Cica-care© were initially compiled in Table 1.

Table 1. Details of different PGF-Biopor®ABs and Cica-care© for testing.

Sample Name	Cica-Care©	PGF-1000-6	PGF-1000-50	PGF-2000-6	PGF-2000-50
Sample size/cm²	32.00	32.00	32.00	32.00	32.00
% of PGF (%)	0.00	42.00	37.00	40.00	35.00
% of Biopor®AB (%)	100.00	58.00	63.00	60.00	65.00
Composite Weight/g	3.26	0.71	0.83	0.72	0.83
Thickness/mm	2.49	0.83	0.85	0.97	0.92
$MIU_{warp,\ weft}$/µm	0.73, 0.76	0.80, 0.80	0.60, 0.67	0.67, 0.72	1.00, 1.00
$MMD_{warp,\ weft}$/µm	0.012, 0.010	0.023, 0.036	0.019, 0.025	0.020, 0.031	0.026, 0.031
$SMD_{warp,\ weft}$/µm	0.26, 0.22	0.90, 5.21	1.57, 3.55	1.42, 6.48	0.53, 2.00
Pore size/µm	No pores	64.53	131.08	38.55	95.65
Number of pores/mm	Not applicable	1.76	1.97	1.33	1.62
WVTR/(g/m²/day)	13.50	141.15	72.66	64.32	138.80

Note: Coefficient of friction (MIU) in surface properties indicates surface roughness. The mean deviation for MIU (MMD) indicates the variation of roughness. The mean absolute deviation for MIU (SMD) indicates geometrical roughness. Water vapor transmission rate (WVTR) measures the property of water permeability and evaluates the barrier properties for the transport of water/vapour/oxygen.

Cells were seeded into 96-well plates at a density of 1×10^5 cells/ml. The L929 cells were cultured in MEM medium with 10% horse serum within a humidified CO_2 incubator (5% CO_2) at 37 °C. According to the international ISO-10993-5 standard, cell viability was assessed at 24-hour and 72-hour intervals following indirect contact with PGF-Biopor®AB in a cell proliferation assay. Each sample was assessed in triplicate, and the resulting purple solution was measured spectrophotometrically. After 24 and 72 h, live and dead cell counts were conducted using a microplate spectrophotometer (BioTekTM, Eon, MPS-02) equipped with a 570 nm filter for calorimetric measurement (reference 650 nm). Cell viability percentage was computed using the following equation:

$$\text{Cell viability (\%)} = \text{Live cells}/(\text{Live cells} + \text{Dead cells}) \times 100\% \quad (1)$$

At the end of 72 h, cell density images were taken using a microscope (Olympus CKX41, MIS-02, Tokyo, Japan).

For the assessment of quantitative surface topologies, the coefficient of friction (MIU), the mean deviation for MIU (MMD), and the mean absolute deviation for MIU (SMD) were obtained using a surface property module of a Kawabata KES-F testing system. The water vapor transmission rate (WVTR) for PGF-Biopor®AB (samples) and Cica-care© (control) was determined following ASTM E96-14 for the water permeability test in the cup method. Each disc-shaped sample of 96 cm^2 was securely mounted on top of a cylindrical cup containing 46 mL of distilled water. The rough side of Biopor®AB (intended for skin contact), was placed downward, facing the water to simulate vapor transfer from the skin to the environment. Three replicates were conducted, and the weight of each prepared sample was recorded before and after every 24 h. The water permeability was calculated using the water vapor transmission rate (WVTR) formula:

$$\text{WVTR} = \text{change in mass}/(\text{area})/(\text{time}), \text{ unit in } g/m^2/day \quad (2)$$

2.4.3. Clinical Scar Assessment

In the trial patient study and non-healed wound study, an assisted transdermal delivery system (ATDDS) was employed to facilitate the self-pumping of PGF-Biopor®AB for PGF-SGS dual therapy, mechanotherapy, and active-fluid transport (Figure 3). In the trial patient study, large-area (>100 cm^2) degree-2 and degree-3 scarring sites (zone 1 and zone 2) were selected from the leg of a burn patient (age 20, 60 Kg, BMI 25). Both the samples and control were extracted from adjacent scarring areas to facilitate straightforward comparison. In a non-healed wound study (age 53, 52 Kg, BMI 21.5), a circular patch was made to ensure a close to 10 mmHg longitudinal pressure for non-healed scar healing. When the scar hypertrophy was completely flattened by PGF-Biopor®AB, an open wound with Silvex® and aloe was applied at the scar maturation stage to complete the scar-healing process. Clinical scar characteristics were evaluated using criteria outlined in our prior report [13]. The assessment included scar color, scar texture, and final outcomes in thickness, pliability, and elasticity, all of which were conducted using the Vancouver Scar Scale.

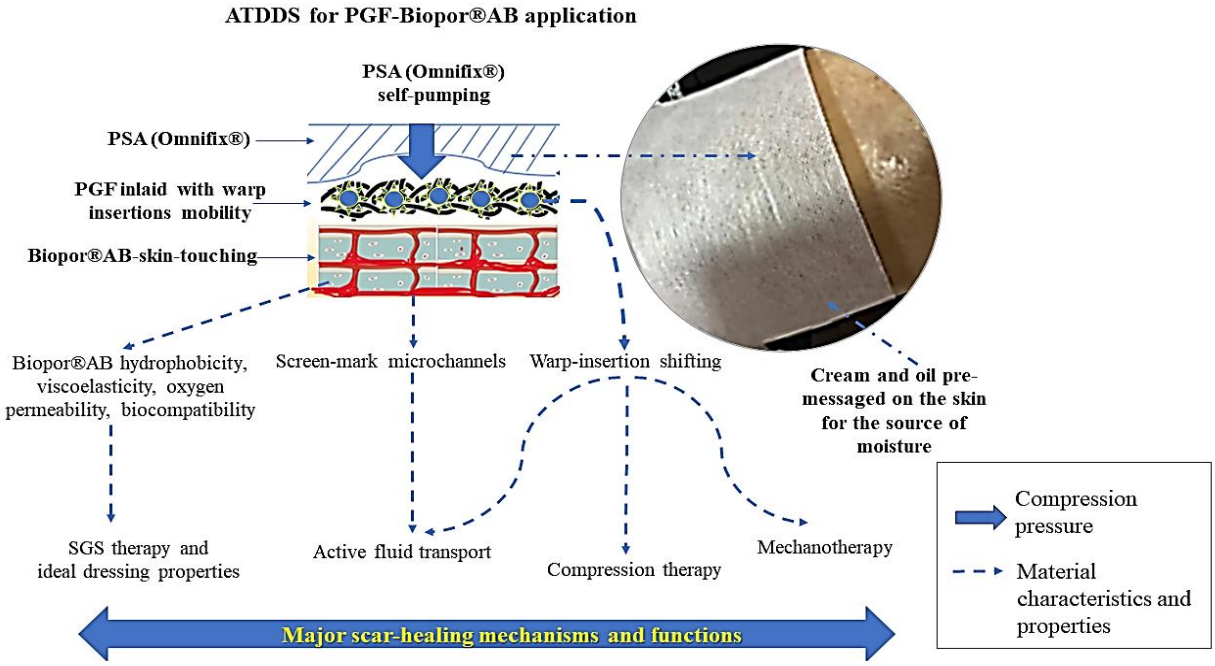

Figure 3. Illustration of an assisted transdermal delivery system (ATDDS) for PGF-Biopor®AB application, attending the major scar-healing mechanism and functions.

3. Results and Discussion

3.1. Vitro Cell Viability by MTT Assay and Analysis

All prepared samples (PGF-1000-6, PGF-2000-6, PGF-1000-50, and PGF-2000-50) were selected based on optimal mechanical properties determined by the Chamis model application [18]. The MTT method was employed to evaluate the impact of varying Biopor®AB printing layers on L929 cell viability. Adhering to the 10993-5 standard of cytotoxicity, a <30% reduction in cell viability induced by PGF-Biopor®AB would be categorised as non-cytotoxic.

PDMS possesses superior flexibility, film-forming ability, biocompatibility, and resistance to chemical degradation, and the use of medical grade silicone Biopor®AB guarantees biocompatibility and is free from allergens for continuous

skin application [19]. As illustrated in Figure 4A, with a recorded <30% reduction in cell viability for both 1 day and 3 days, all samples were confirmed non-cytotoxic, ensuring their safety for patient use in continuous 3-day applications. When examining cell viability (%) over time (cultured for 1 day and 3 days), all samples exhibited a trend of increasing cell viability (Figure 4A). In the case of thin-layer samples (PGF-1000-6 and PGF-2000-6), they initially displayed lower cell viability on day 1 but ultimately reached nearly 100% cell viability by the end of 3 days. This robust cell viability, comparable to commercial SGS (Cica-care©), suggests vigorous cellular activities for repair and regeneration, representing an optimal outcome for scar healing. In contrast, thick-layer samples (PGF-1000-50 and PGF-2000-50) also started with lower cell viability on day 1 but concluded with lower cell viability than commercial SGS (Cica-care©) by the end of 3 days, still achieving over 70% cell viability. To quantify and visually represent the rate of cell proliferation on different PGF-Biopor®AB samples and Cica-care©, microscopic images were captured at the end of day 3. Intriguingly, images depicting both high and low cell densities coexisted within the range of above 70% cell viability (Figure 4B).

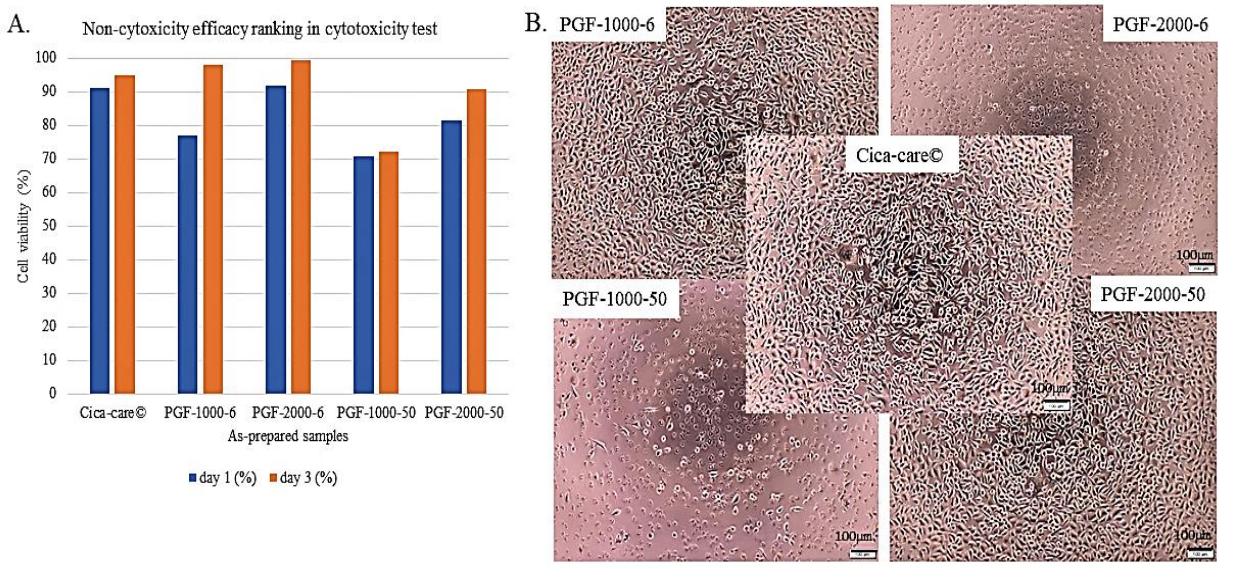

Figure 4. Results of cell viability in cytotoxicity test: (**A**) Efficacy ranking by cell viability (%) at the end of day 1 and day 3, comparisons of tested samples at 25% concentration (>70% is considered as non-cytotoxic.); (**B**) Microscopical images of cell density at the end of day 3.

Among samples exhibiting >30% reduction in cell viability, both PGF-1000-6 and PGF-2000-50 demonstrated nearly identical extents of high cell density, similar to the Cica-care© control (designated as "high cell density"). Microscopic images revealed that cell spreading with an elongated shape indicated robust cellular alignment and migration, signifying the potential for cellular growth and proliferation prohibition in the context of repair and regeneration. The "high cell density" samples, with close to 100% cell viability and comparable cell density to the commercial SGS control (Cica-care©), suggest an effective outcome in scar healing performance.

Conversely, PGF-2000-6 and PGF-1000-50 displayed a lower rate of cell density (designated as "low cell density" samples). Furthermore, cells in these samples appeared more circular in microscopic images, indicating lower cellular activities. The coexistence of both high and low cell density in samples with >30% reduction in cell viability indicates that the percentage of cell viability is not directly proportional to the extent of cell density. Given the absence of literature data for scar therapeutics' performance reference concerning high and low cell density samples, utilizing both types of samples in patient trials becomes necessary.

Scar healing is a complex physiological process involving cell viability performance in various aspects such as alignment, movement, migration, and proliferation [20]. Studies have shown that substrate characteristics, including materials, topography, and stiffness, can influence cell behaviour [21]. According to Wu et al.'s study on PDMS surface topography, micro- and nanoscale morphological features in pattern spacing and depth guide cell alignment and migration [21]. Curtis et al. have highlighted the impact of cell tension at topography and topography-induced strain on cellular movement, shape, orientation, and polarity of movement [22]. The guidance of endothelial cells in angiogenesis and regenerating tissues is influenced by both physical guidance (topographic and mechanical) and chemical guidance (adhesive) [22]. Per Ross Harison, topographic reactions are biocompatibility-related [23], with cells exhibiting contact

guidance and topographic guidance in regions of extreme curvature [22]. Scar healing of PGF-Biopor®AB addresses inflammation, fibrosis, and angiogenesis. Cross-linking silicone Biopor®AB with hydrophobic SiO_2 provides sufficient chain mobility, stretchability, and low surface energy that improves the bonding between PGF and Biopor®AB [23]. Hydrophobicity and high adhesion of Biopor®AB surface reorganize patterns of screen gauge to build cellular-accessible Biopor®AB microchannels and modify the PGF-Biopor®AB surface structural features [24]. The anisotropic characteristics and Biopor®AB microchannels construct a favorable microenvironment for scar healing therapeutics (Figure 5a,b). Thus, the PGF-Biopor®AB structure promotes cell movement, adhesion, and alignment through microscale spaces, facilitating cell growth and proliferation exhibition, ultimately contributing to tissue repair and regeneration for scar therapeutics (Figure 5c).

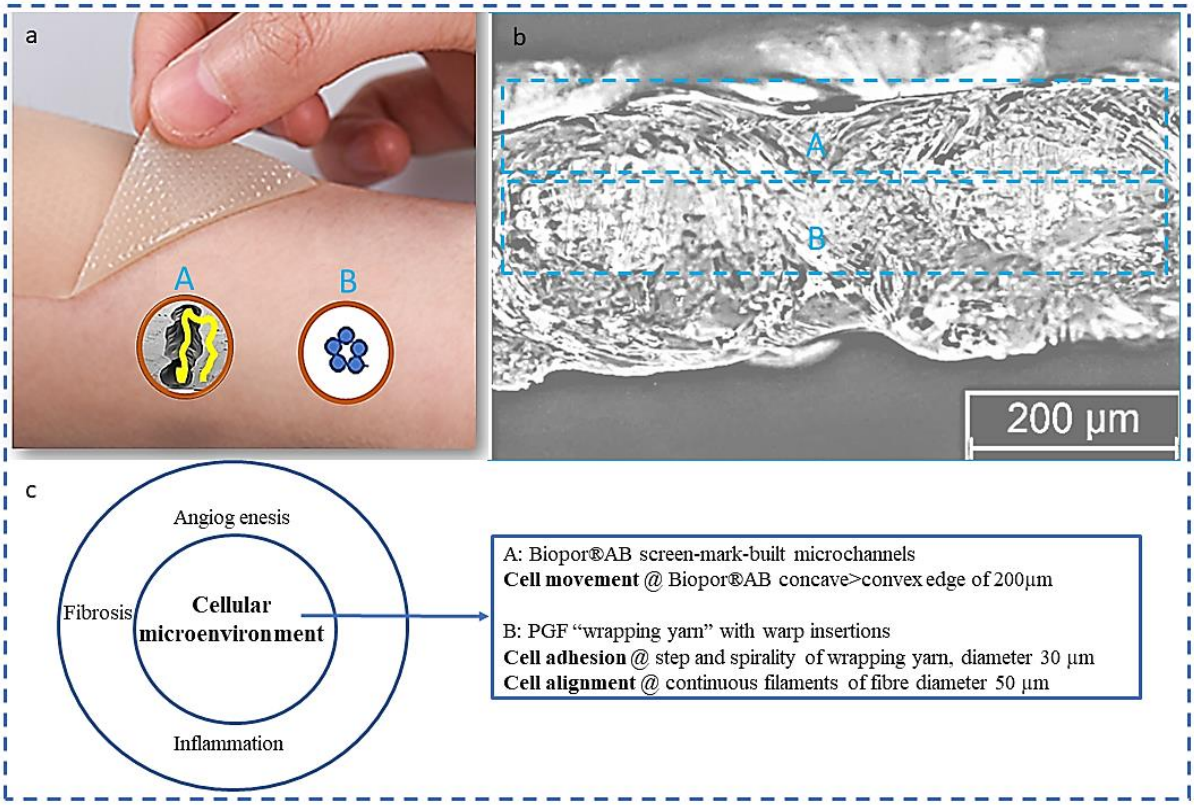

Figure 5. The microscale spaces within the PGF-Biopor®AB structure construct the scar-healing microenvironment addressing inflammation, fibrosis, and angiogenesis, scar inhibited by Biopor®AB and PGF surface anisotropic characteristics. (**a**) Bandaging pressure-application of PGF-Biopor®AB on the skin (A—Surface microchannel structure, microchannels provide pathways of cellular transport; B—PGF "Through-the-thickness" structure). (**b**) Microscopic cross-section of PGF-Biopor®AB (A—Surface microchannel structure, B—PGF "Through-the-thickness" structure). (**c**) PGF-Biopor®AB with different microfeatures creates a cellular microenvironment, addressing scar healing against inflammation, fibrosis, and angiogenesis.

The development of surface anisotropic characteristics in PGF-Biopor®AB encompasses considerations of viscoelastic properties, roughness, and rigidity. These topological features play a crucial role in influencing cell-surface interactions, thereby impacting cellular physical guidance. Figure 6A depicts the construction of surface structure with screen-marked microchannels. Within this structure (Figure 6B), a concave > convex edge with approximately 200 μm was observed. In the PGF-inlaid "through-the-thickness" structure (Figure 6C), continuous filaments of fibre diameter 50 μm each were observed (Figure 6D). In the PGF-inlaid "through-the-thickness" structure, step and spirality of wrapping yarn built micro features of diameter 30 μm each (Figure 6E).

According to literature data, The microscale fibre structure influences cell alignment, cell orientation and cell contact inhibition [22,23,25]. Fibres with a radius of 50 to 230 μm provide sites for cell alignment, cells can move on such concave > convex edges and align on the inside of a bend [22]. Cell orientation and contact inhibition occur on fibres with a radius of 15–20 μm, and cells spread and orient themselves at <50 μm radii of curvature [22]. According to Jiang et al., bending a PDMS slab can create surface waves that induce mechanical stress for contact guidance, and cells can elongate and spread parallel to the direction of surface waves of >8 μm [25]. Referencing such microstructural data, the observed PGF and Biopor®AB-coated micro-dimensions in PGF-Biopor®AB structure fit cellular activities

of cell alignment, cell movement, and cell adhesion. Similar to the structural design of a 3D hybrid scaffold, the controllable fibre micro-dimension from PGF and the increased surface-to-volume ratio from screen-printed microchannels can ameliorate cell adhesion, proliferation, and differentiation [26]. Good adhesion from the pressure-screen-printed matrix–fibre interface guarantees good stress transfer from the soft matrix to the stiff fibre, a proper stress transfer of tissue-tension-off-loading mechanical performance for scar therapeutics [27,28].

In addition to the surface anisotropic characteristics, the inherent 100% oxygen permeability from Biopor®AB further enhances the availability of oxygen species, favouring cell adhesion [13]. When cells respond to mechanical anisotropy, the adhesive-viscoelastic surface of PGF-Biopor®AB is sufficiently isotropic to be deformable, enabling cells to exert significant traction, hindering their ability to move, and spread. This viscoelasticity is mechanically analogous to cells grown on spheres with sufficiently small radii of curvature, causing cells to be trapped by PGF-Biopor®AB isotropic curvature and resulting in approximately 30% inhibition of cell viability. This also clarifies why, despite small topographical differences between samples (refer to Table 1 and Figure 4), there is a notable discrepancy in cell density, leading to the classification of samples as high- or low-density. Under pressure-induced compression with warp-insertion shifting, Biopor®AB viscoelasticity allows the bending of such micro features, and the creation of surface waves as that of the PDMS slab induces mechanical stress for contact guidance. Essentially, the construction of micro features and PDMS surface anisotropic characteristics in PGF-Biopor®AB constructs a breathable dressing with surface hydrophobicity [9]. This unique surface hydrophobicity with breathability supports robust cellular activities and barrier properties, facilitating cell growth and proliferation exhibition, thereby fulfilling the optimization goals for multi-scar-healing efficacy.

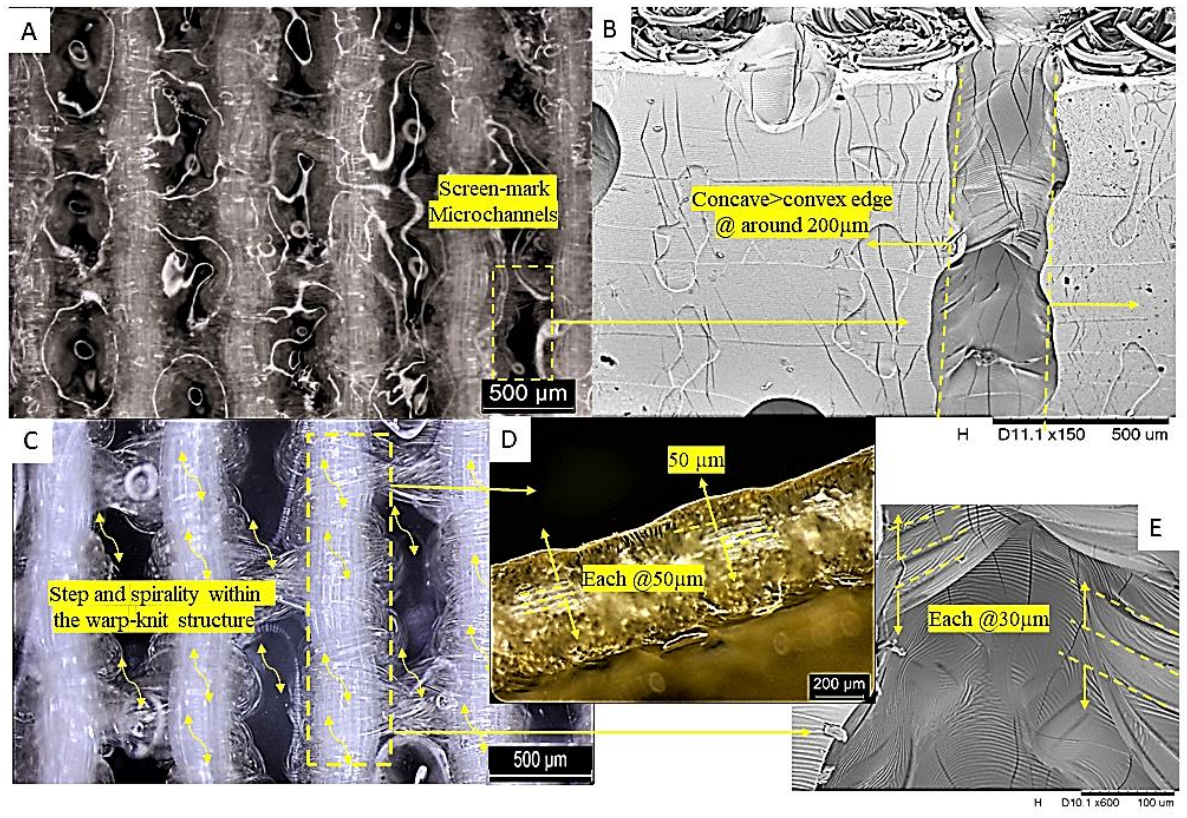

Figure 6. Scar-healing surface anisotropic characteristics for PGF-Biopor®AB: (**A**) screen-mark-microchannel-built surface structure, (**B**) Concave>convex edge @microchannels, (**C**) PGF-inlaid "through-the-thickness" structure, (**D**) Fibre diameter of continuous filaments, (**E**) Steps and spirality in the warp-knit structure.

The major cause of hypertrophic scar formation is the excessive proliferation of fibroblasts that causes excess collagen deposition. Drawing insights from surface characteristic studies in scar healing literature, it is suggested that fibroblasts grow on the surface of anisotropic structured patches, promoting cell growth while inhibiting cellular proliferation without a negative effect on cell viability [2]. In the PGF-Biopor®AB scar-healing microenvironment, cell viability (%) serves as an indicator of cellular behaviors related to alignment, movement, adhesion, and proliferation. The anisotropic characteristics of PGF-Biopor®AB and microscale surface anisotropic features should encourage cell growth while same time inhibiting cellular proliferation. The inhibiting excess proliferation of fibroblasts indicates

reduced collagen production and cell growth with cell proliferation reduction (without obvious toxicity) reflects potential values of scar inhibition. Therefore, >70% cell viability and the extent of cell density should correlate with corresponding scar healing performance in a patient study. Since cell density images from cell culture can only be qualitatively categorized as high or low and are not quantifiable for analysis, the subsequent in-depth study on surface characteristics and cell viability analysis will focus solely on cell viability (%). By examining the impact of viscoelastic properties, roughness, and rigidity on cell viability (%), the aim is to establish a reference guideline for PDMS surface characteristics in the context of scar therapeutics.

3.2. Trial Patient Study with Non-Healed Wound and Scarring Tissues

In addressing non-healed wounds, many multifunctional biodegradable biomaterials have been developed and used in wound care to achieve the functions of inhibiting bacterial growth, promoting angiogenesis, and accelerating healing [2,29,30]. However, the use of such biodegradable biomaterials and silicone products in non-healed scarring wounds is still not suggested by plastic surgeons for problems of ulcers and abnormal hypertrophies. Stretching the polymer inverse opal patterns in an ellipsoidal porous patch signified the function and possibility of anisotropic cell-inducing ability for scar inhibition [30]. To achieve earlier tissue regeneration and overcome the formation of scars during wound healing, PGF-Biopor®AB equips a microchannel structure with high WVTR and the operation of low-pressure incorporation with viscoelasticity helps in avoiding the formation of hypertrophic scars.

In the non-healed wound study, a practical trial involving a patient with a degree-2 non-healed scarring wound was conducted over 7 days (Figure 7a,b). Cutting PGF-Biopor®AB and Omnifix© in a circular shape ensured longitudinal, lowest, and consistent pressure application (<10 mmHg) to avoid pressure-induced skin ulcer and hypertrophy. After pressure release by viscoelasticity of Biopor®AB, the scar became flattened with no scabs on day 3. Figure 7bi–biv shows the progress of hypertrophy reduction, with no hypertrophy after 3 days of PGF-Biopor®AB application. 10 days post-injured wounds are in the healing stage of proliferation (Figure 8), a condition of high demands of WVTR from 1900–2109 g/m^2/Day [31]. As insufficient WVTR would result in recurring inflammation and delayed healing, open wound healing was administrated with silvex® and aloe upon no hypertrophy. The open wound with aloe ensured sufficient WVTR and the use of silvex® ensured no recurrence of inflammation, both addressing proper/scarless wound healing. PGF-Biopor®AB application got rid of the hypertrophy in 3 days; sufficient WVTR at the healing wound for angiogenesis and silvex® and aloe prevented the recurrence of inflammation. No non-healed scarring wounds, no scabs, and no progressing hypertrophy were found within 7 days, which were evident in an earlier-scarless healed wound (Figure 7bv). No surface hypertrophy and no scabs within 7 days indicate that PGF-Biopor®AB significantly inhibited the formation of scars and helped reduce the wound-healing time. Larger Biopor®AB surface area (from fillers in Biopor®AB) and active delivery characteristics of 3D channel structures are conducive to increasing adhesion sites for cell growth and infiltration, favouring the early healing of non-healed scarring wounds [32]. In accelerated wound repair, the aligned microstructures should provide direct guidance for cellular growth orientation and extension [26]. Further, proper longitudinal pressure incorporation with sufficient ventilation performs the functions of inhibiting excess fibroblast proliferation and reducing collagen production. As a result, enhanced migration and proliferation of surrounding fibroblasts are conducive to early wound closure and a healed wound without scar in the early stage of wound healing. However, due to complications of non-healed scarring wounds, the use of PGF-Biopor®AB on large areas of non-healed scarring wounds should be under the supervision of plastic surgeons.

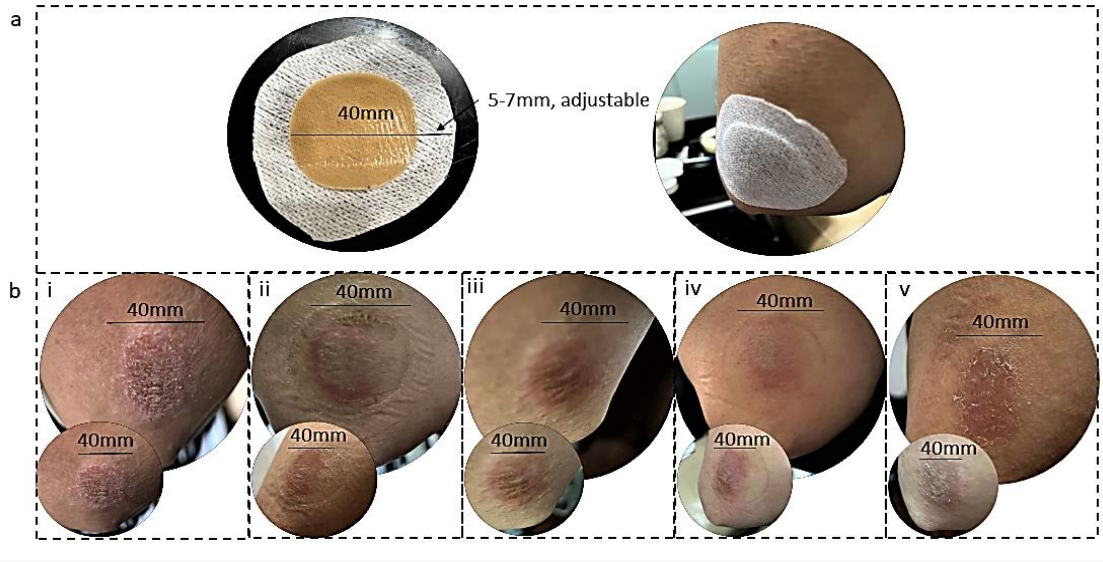

Figure 7. Non-healed wound study in ATDDS for PGF-Biopor®AB application by K.C. Lui, with 40 mm non-healed wound of degree 2 from day 1-day 7: (**a**) Circular-cut PGF-Biopor®AB and Omnifix© to the same size as a wound, adjustable size from 5–7 mm for consistent and lowest pressure to the comfort of application. (**b**) Imaging treatment efficacy from day 1, 2, 3 and day 7: **i.** Initial condition, **ii**. Day 1, **iii**. Day 2, **iv.** Day 3 and **v**. Day 7.

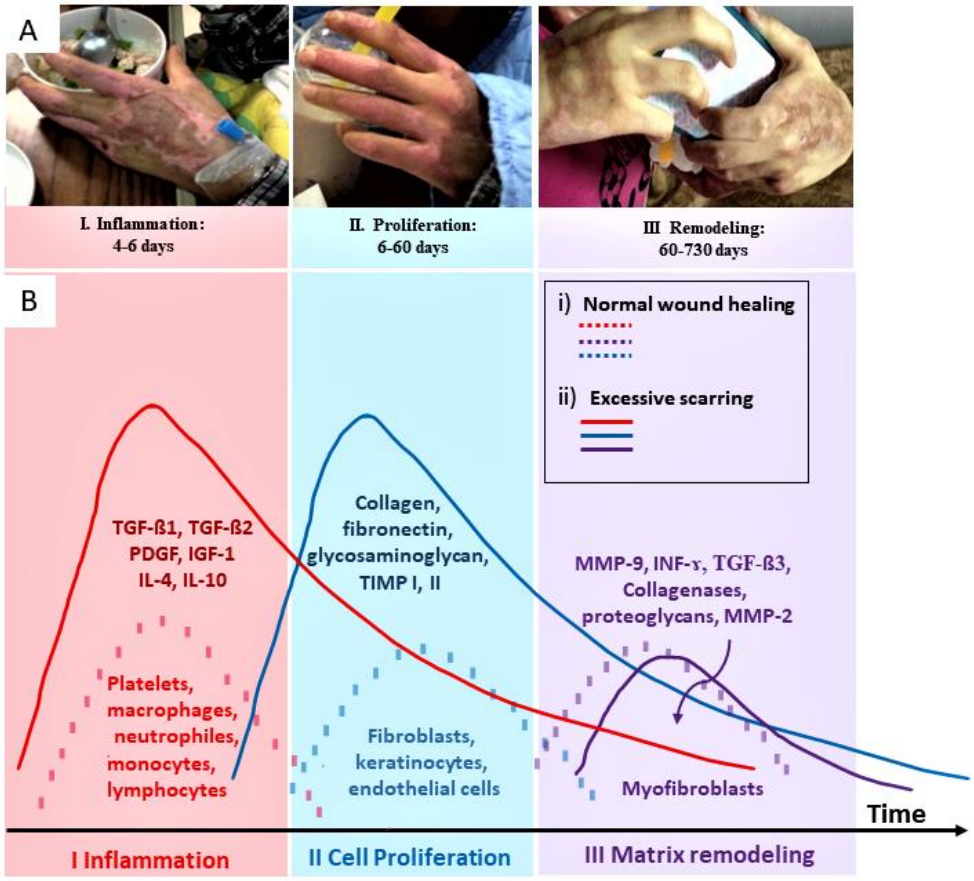

Figure 8. (**A**) Illustrative photographs of the three stages of wound healing (self-sourced, with permission, from the long-term hand wound healing of *Ms Carman Chong*), and (**B**) Changes during the stages of inflammation, cell proliferation and matrix remodelling from (i) Normal wound healing to (ii) Excessive scarring over time (Reprinted with permission from reference [33] copyright 2011 Springer)

A practical trial involving a patient with degree-2 and degree-3 scarring tissues was conducted over one month, utilizing Vancouver Scar Scale parameters (Figure 9). Significant improvements in surface irregularity were noted, particularly along the scar edges, indicating a reduction in irregularities. Scar thickness investigation revealed a decrease

in hypertrophy, with a notable thinning of the superficial scar. In terms of pliability, the scar structure exhibited increased smoothness and enhanced elasticity, transitioning from thicker to finer elastic fibres. Pigmentation also showed a slight reduction in colour. Compared to literature data, typical efficacy for SGS involves wearing it over the scar for 12–24 h per day for at least 2–3 months, while PGT typically shows efficacy over 6 months [34,35]. Thus, the over 70% cell viability echoing one-month efficacy in the PGF-Biopor®AB application confirmed optimization of efficacy through PGF-SGS dual therapy, mechanotherapy, and active-fluid transport. The improvement in surface irregularities, scar thickness reduction, and enhanced overall scar elasticity in shorter treatment time indicate a synergistic effect of multi-therapeutic efficacy. The sustained dynamic hydration performance observed in WVTR, and water uptake capability in previous research further support active-fluid transport, supporting overall scar improvement [13].

In the suggested assisted transdermal delivery system (ATDDS) for PGF-Biopor®AB application, the drug layer containing Aveeno® functions as an effective occlusive-diffusion-penetration source for water hydration. The continuous pressure-driven self-pumping activates warp insertion shifting, facilitating dynamic and sustainable diffusional transport of Aveeno® with water (fluid) in the cellular accessible 3-D channel structure. At a cellular level, the asymmetric "spiral-through-the-thickness" structure with screen-mark microchannels aids effective directional transport, and current >70% cell viability evidenced their accessibility to positive cellular activities [13].

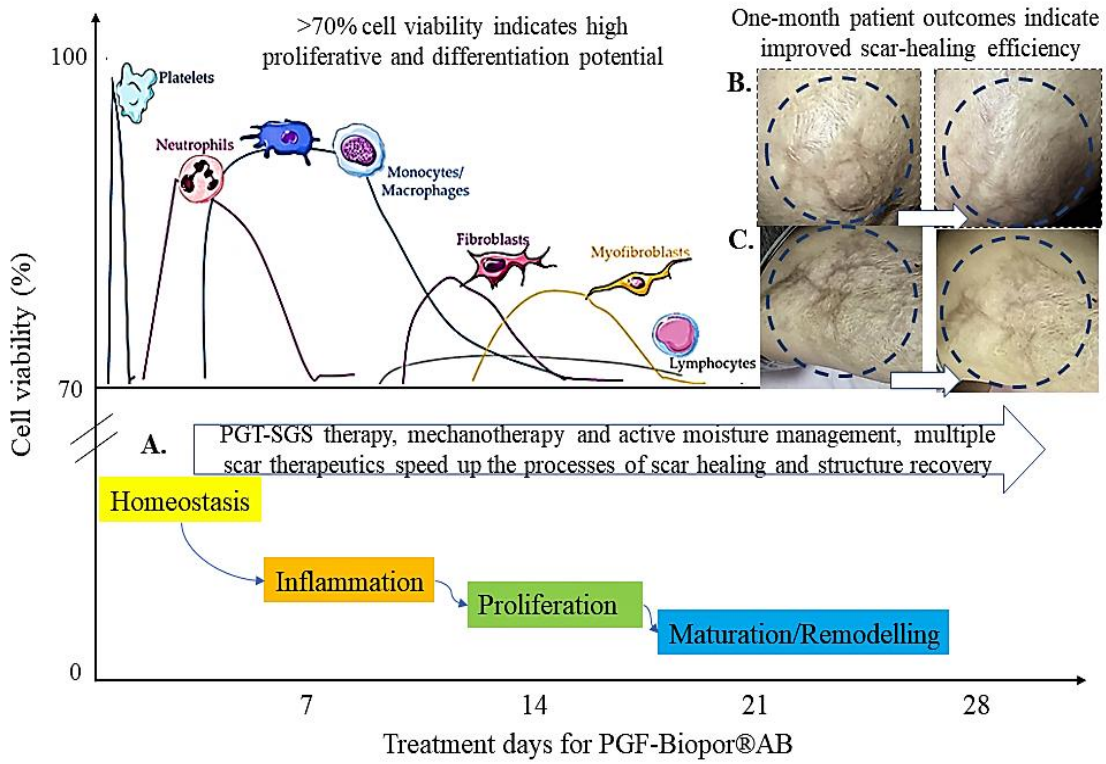

Figure 9. Scar-healing roles of PGF-Biopor®AB in positive cell viability and treatment, summarizing cell viability (%) against the result of a trial patient study in ATDDS for PGF-Biopor®AB application on a burn patient (Carman Chong) with two zones of degree 2 and degree 3 scarring tissues from day 1-day 28, imaging treatment efficacy from day 1 and day 28: (**A**) Healing processes, (**B**) Zone 1 (with PGF-1000-50), and (**C**) Zone 2 (with PGF-1000-6) (Reprinted with permission from reference [13] copyright 2023 MDPI).

For studying the influence of relative surface roughness (MIU, MMD and SMD) and the influence of stiffness on cell viability, the related parameters were analysed (Table 1). Both the MIU_{warp} and MIU_{weft} enhancements supported cell viability (%) increase and a range of MIU from 0.6-1 favoured >70% cell viability. A range of MMD above 0.01 and a range of SMD_{warp} from 0.2 to 1.6 and SMD_{weft} from 0.2 to 6 favoured >70% cell viability. Referencing roughness configurations of smaller cells in nanoscale 10–102 nm (take vein endothelial cells as an example), the above PGF-Biopor®AB $_{SMD}$ is equivalent to around 176–4000 times larger surfaces. Here, the high PGF-Biopor®AB $_{SMD}$ means the availability of more cell adsorption sites and the provision of sufficient space for cellular activities [36]. Here, high PGF-Biopor®AB $_{MIU/MMD/SMD}$ is equivalent to the provision of large adsorption sites for bioactive molecules, and the geometrically rougher surfaces enable a higher ability of cell adhesion, growth, and differentiation [36]. The rougher surface with high MIU, MMD and SMD provides a larger solid−liquid interface area, the results of over 70% cell

viability indicated high cell growth and differentiation potential in a favourable scar-healing microenvironment [37]. Over 70% cell viability in all selected samples supported not only the scar-healing efficacy of overall scar improvement but also cellularly assessed the functionality of fluid transport microchannels in the 3D channel structure.

Referring to the seven elements of the Arzt heptahedron for skin hydration, the mechanical behaviour of both a-keratin and b-keratin of the skin relies heavily on the degree of hydration [35,37–39]. Increasing hydration reduces scar tissue stiffness and modulus as the keratin matrix absorbs moisture [36–39]. Thus, adequate hydration strives to restore collagen tensile strength and elongation in scar tissue for earlier scar maturation [38]. The surface anisotropic characteristics and microscale scar-healing microenvironment all favour cell alignment, adhesion, movement, and proliferation. Here, active-fluid transport strived for adequate hydration, and dual PGF-SGS therapy and mechanotherapy enabled the reorganization of collagen and elastic fibre networks, fulfilling the scar-healing role of scar structure recovery. Concluding from both cell viability and trial patient study results, using a sample of over 70% cell viability, with either low cell density (PGF-1000-50) or high cell density (PGF-1000-6) achieved the same one-month efficacy. This one-month efficacy of both PGF-1000-6 and PGF-1000-50 implies that >70% cell viability can be a sufficient scar healing therapeutic guideline for PDMS composite. Over 70% cell viability is sufficient to achieve scar therapeutics, regardless of low or high cell density. The one-month efficacy results align with the findings of the cell viability study, supporting the above active silicone occlusive healing theory with multi-therapeutics from compression-silicone dual therapy, mechanotherapy, and active-fluid transport.

3.3. Possible PGF-Biopor®AB Scar Healing Mechanism

Figure 10 illustrates the Ichikawa diagram elucidating scar-healing functions and associated mechanisms. Optimizing scar healing efficacy involves three key functions: (i) PGF-SGS dual therapy, (ii) Mechanotherapy incorporating tension-shielding and pressure redistribution, and (iii) Active moisture management. In PGF-SGS dual therapy, SGS therapy is conducted through Biopor®AB-skin contact with Biopor®AB exposure at the outer surface of PGF-Biopor®AB. Medical silicone Biopor®AB performs SGS therapy with inherent characteristics of oxygen permeability and occlusive hydration [13]. The pressure-driven “warp insertions” mobility design accomplishes compression therapy via “warp insertions” shifting to achieve PGF-SGS dual therapy.

Collagen fibrils in scarring tissue are arranged in non-parallel arrays and not in alignment with the lines of tension but are sensitive to the local stress profile. The organization of collagen fibrils is also highly reconfigurable, collagen tissues show a nonlinear stress response (stress-stiffening): collagenous tissues stiffen as they are strained (by an external force) [40]. Biopor®AB is composed of at least two polymer networks in PDMS and PVMS. When PDMS/PVMS combined with PGF-textile reinforcement from screen printing, elastic gradient tunability for tensile and shear (from PDMS/PVMS) exhibited high strength and diverse shape transformation ability (Figure 11). Elastic gradient tunability allowed a change from isotropic to anisotropic within the Biopor®AB screen-mark microchannels.

PGF-Biopor®AB would become softened when stretched to allow pressure and tension reduction, which fits well with the stress-stiffening properties of collagen, causing a reduction in collagen deposition for less scarring. The Biopor®AB silicone characteristics of oxygen permeability and occlusive hydration also allow water vapor penetration, oxygen penetration, and stratum corneum hydration, demonstrating scar repair function. The oxygen permeability in Biopor®AB provides an oxygen environment that supports reactive oxygen species for the sustained release of pro-inflammatory cytokines. The coexistence of hydrophobicity and permeability, the building of micro hierarchy structure for liquid collection and directional movement, on the other hand, resists bacteria invasion and reduces infection, stopping continuous infections and excess inflammation [9,13,41–43].

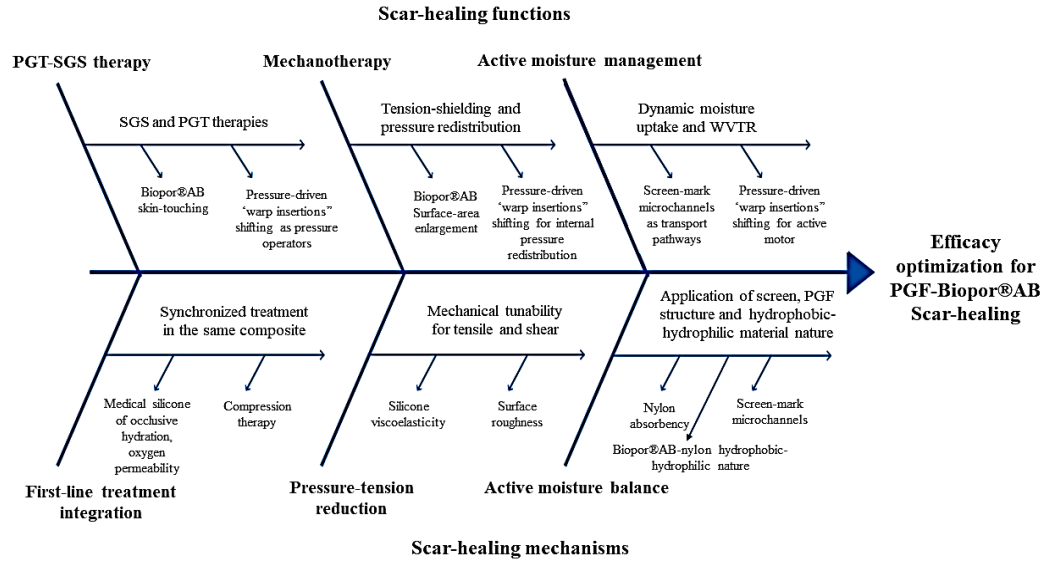

Figure 10. Ichikawa diagram illustrating possible scar-healing functions and mechanisms of PGF-Biopor®AB.

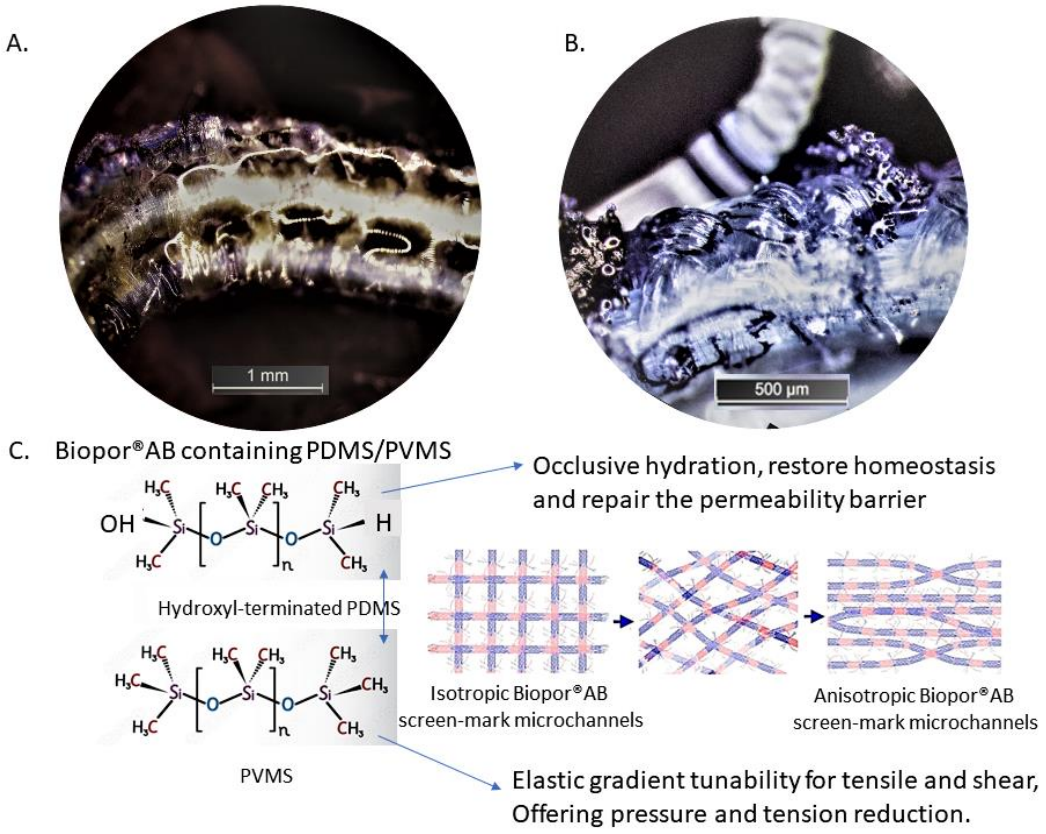

Figure 11. Biopor®AB scar-healing functions: (**A**) PGF-Biopor®AB under compression; microscale features curve up; (**B**) Dyed effective pathways shown effective diffusion; (**C**) Biopor®AB containing PDMS and PVMS, hydroxyl-terminated PDMS performs occlusive hydration and PVMS performs elastic gradient tunability.

The Biopor®AB-nylon characteristics in the "warp insertions" mobility design offered higher water-holding capacity, enhanced transdermal water loss and normalized the barrier function. This result of >70% cell viability demonstrates excellent biocompatibility, high cell viability, and proliferation capacity, the one-month scar-healing efficacy and an early scarless healed wound signified the appropriateness in the magnitude of occlusive hydration. The results of cell viability and patient outcomes reflected stimulation of cell growth and proliferation inhibition—elastic gradient tunability reduced collagen deposition while occlusive hydration reduced hypertrophy by keratinocyte hydration, both restoring the homeostasis of the barrier function and correcting the defective permeability.

Optimizing scar healing efficacy involves three primary mechanisms (Figure 10): (i) Integrating and synchronizing PGF and SGS therapies to expedite the scar-healing process, (ii) Reducing tension through viscoelasticity and redistributing pressure via tension-shielding, and (iii) Enhancing permeability through active water uptake for effective moisture management. Addressing the water non-permeability of SGS and mitigating pressure points from PGF, PGF-Biopor®AB harmonizes the benefits of both therapies and eliminates such problems, realizing compression-silicone dual therapy in the first place.

Mechanotherapy involves leveraging viscoelastic properties at the structural level, and pressure-driven PGF-Biopor®AB enhances the surface area of Biopor®AB and facilitates warp insertions shifting for tension-shielding and pressure-redistribution [43]. Subsequently, applying viscoelasticity and surface roughness contributes to mechanotherapy, aiding in pressure and tension reduction. Notably, the surface roughness created by the Biopor®AB screen-mark microchannels promotes tension shielding and pressure redistribution. The "warp insertions" shifting, propelled by pressure, generates internal pressure redistribution, collectively supporting mechanotherapy.

For active moisture management, the screen-mark microchannels form cellular-accessible pathways for transport, and the "warp insertions" mobility design serves as pressure-driven "pressure operators" for efficient nylon absorbency, enabling water absorption with retention for effective moisture control. Validation through human skin WVTR and 13% water uptake confirmed that the PGF-Biopor®AB microchannel structure was an effective permeability barrier, normalising the barrier function [13]. The microchannels, shaped by screen-mark structures, facilitated the diffusion of water and nutrients from applied creams and oils onto scarred tissues, ensuring both ample moisture for the function of transdermal drug delivery and the construction of an occlusive microenvironment conducive to skin repair and regeneration.

These three mechanisms collectively support the core functions of scar healing, resulting in one-month scar-healing efficacy and 7-day scarless-healed wound. The microchannels serve as effective pathways for micro and nanocarriers, contributing to inflammation inhibition and enhanced angiogenesis against fibrosis in the various stages of scar healing. The ability of water-retaining in microchannel structure provides a moist microenvironment crucial for maintaining a balance between collagen progress and lysis, thereby promoting rapid scar inhibition. The PGF-Biopor®AB system excels in water absorption with retention, ensuring effective moisture control.

4. Conclusions

An innovative biaxially screen-printed textile-reinforced composite, PGF-Biopor®AB, was developed as a highly effective scar-healing dressing. Samples from the PGF-Biopor®AB series, distinguished by optimal mechanical properties, consistently demonstrated >70% cell viability across all scenarios. The confirmation of non-cytotoxicity, adhering to the 3-day ISO-10993-5 standard, substantiated the safety of a continuous 3-day patient usage for PGF-Biopor®AB. Patient outcomes over one month and a 7-day scarless-healed wound validated the effectiveness of multifaced scar-healing optimization strategies, reinforcing the proposed scar-healing functions and mechanisms.

Surface characteristic analyses revealed that the incorporation of Biopor®AB into PGF resulted in improved tensile and shear moduli, increased roughness, and enhanced mechanical stiffness. These improved surface characteristics, stemming from optimal mechanical properties, favored the attainment of >70% cell viability. The inclusion of both low and high-cell-density samples in the patient study demonstrated comparable one-month scar-healing efficacy and a 7-day scarless-healed wound, suggesting that >70% cell viability is sufficient for optimal scar therapeutics, regardless of cell density levels or cell-culture conditions. The results of >70% cell viability indicated enhanced cell growth and proliferation inhibition, showcasing the multi-therapeutic potential of scar healing. Therefore, >70% cell viability can be established as a guideline for PDMS in scar healing efficacy.

In summary, PGF-Biopor®AB facilitated the repair of hypertrophic scars through compression-silicone dual therapy, mechanotherapy, and active moisture management. This study introduced a novel perspective on the mechanisms underlying primary scar-healing functions, providing valuable insights for future research in scar-healing materials.

Acknowledgements

The first author would like to thank The Hong Kong Polytechnic University for a 4-year full-time research scholarship. Our special thanks go to Nuruzzaman Noor, Bin Fei and Akanksha Pragya for their contributions to the initial work. X.W. acknowledges research support from the Research Centre of Textiles for Future Fashion and the Research Institute for Sports Science and Technology at the Hong Kong Polytechnic University. Support from the Hong Kong Jockey Club Charities Trust is also acknowledged.

Author Contributions

K.-C.L.: Methodology, Data validation, formal analysis and investigation, Writing—original draft. X.W., C.-w. K.: Supervision and Conceptualization, Writing—review & editing

Ethics Statement

Ethical review and approval were waived for this study, due to self-testing on the non-healed wound performed by Lui Kam Che.

Informed Consent Statement

Informed consent was obtained from all subjects involved in the study.

Funding

We acknowledge research support from the Research Centre of Textiles for Future Fashion and the Research Institute for Sports Science and Technology at the Hong Kong Polytechnic University.

Declaration of Competing Interest

The authors declare that they have no known competing financial interests or personal relationships that could have appeared to influence the work reported in this paper.

References

1. Curtis AS. Cell contacts: Some physical considerations. *Am. Nat.* **1960**, *94*, 37–56.
2. Weng W, Chi J, Wang X, Shi K, Ye F, Zhao Y. Ellipsoidal porous patch with anisotropic cell inducing ability for inhibiting skin scar formation. *Eng. Regen.* **2022**, *3*, 262–269.
3. Cordeiro JM, Nagay BE, Dini C, Souza JG, Rangel EC, da Cruz NC, et al. Copper source determines chemistry and topography of implant coatings to optimally couple cellular responses and antibacterial activity. *Biomater. Adv.* **2022**, *134*, 112550.
4. Martin P. Wound healing—Aiming for perfect skin regeneration. *Science* **1997**, *276*, 75–81.
5. Adan A, Kiraz Y, Baran Y. Cell proliferation and cytotoxicity assays. *Curr. Pharm. Biotechnol.* **2016**, *17*, 1213–1221.
6. Van Meerloo J, Kaspers GJ, Cloos J. Cell sensitivity assays: The MTT assay. In *Cancer Cell Culture: Methods and Protocols*, 2nd ed; Ian AC, Ed.; Springer: Jersey City, NJ, USA, 2011; volume 731, pp. 237–245.
7. Ghasemi M, Turnbull T, Sebastian S, Kempson I. The MTT assay: Utility, limitations, pitfalls, and interpretation in bulk and single-cell analysis. *IJMS* **2021**, *22*, 1–30.
8. International Organization for Standardization (ISO) 10993-5. Part 5: Tests for in vitro cytotoxicity. In *Biological Evaluation of Medical Devices*; 3rd ed.; American National Standards Institute (ANSI): Washington, DC, USA, 2009.
9. Li M, Dong Y, Wang M, Lu X, Li X, Yu J, et al. Hydrogel/nanofibrous membrane composites with enhanced water retention, stretchability, and self-healing capability for wound healing. *Compos. Part B Eng.* **2023**, *257*, 110672.
10. Piel M, Théry M. *Micropatterning in Cell Biology, Part C (Chapter 3)*; Elsevier: Amsterdam, The Netherlands, 2014.
11. Meyers MA, Chen PY. *Biological Materials Science: Biological Materials, Bioinspired Materials, and Biomaterials*; Cambridge University Press: Cambridge, UK, 2014.
12. Meyers MA, Chen PY, Lin AYM, Seki Y. Biological materials: structure and mechanical properties. *Prog. Mater. Sci.* **2008**, *53*, 1–206.
13. Lui KC, Noor N, Kan CW, Wang X. A self-pumping composite dressing improved hypertrophic scar healing with dual therapy and active-fluid transport. *J. Compos. Sci.* **2023**, *7*, 1–21.
14. Ly NG, Denby EF. A CSIRO inter-laboratory trial of the KES-F for measuring fabric properties. *J. Text. Inst.* **1988**, *79*, 198–219.
15. McNeely MR, Sputea MK, Tusneem NA, Oliphant AR. Sample processing with hydrophobic microfluidics. *J. Assoc. Lab. Autom.* **1999**, *4*, 30–33.
16. Hong S, Minary-Jolandan M, Naraghi M. Controlling the wettability and adhesion of carbon fibres with polymer interfaces via grafted nanofibers. *Compos. Sci. Technol.* **2015**, *117*, 130–138.
17. Andersson CH, Dartman T, Gredinger P, Asplund J, Strandqvist H. Flexible composites, strength, deformation, and fracture processes, 1. reinforcement structures and tensile strength. *Mech. Compos. Mater.* **1998**, *34*, 525–536.
18. Chamis CC. Simplified composite micromechanics for predicting microstresses. *J. Reinf. Plast. Compos.* **1987**, *6*, 268–289.
19. Deriabin KV, Kirichenko SO, Lopachev AV, Sysoev Y, Musienko PE, Islamova RM. Ferrocenyl-containing silicone nanocomposites as materials for neuronal interfaces. *Compos. Part B Eng.* **2022**, *236*, 109838.

20. Zhou S, Wang Q, Yang W, Wang L, Wang J, You R, et al. Development of a bioactive silk fibroin bilayer scaffold for wound healing and scar inhibition. *Int. J. Biol. Macromol.* **2024**, *255*, 128350.
21. Wu TH, Li CH, Tang MJ, Liang JI, Chen CH, Yeh ML. Migration speed and directionality switch of normal epithelial cells after TGF-β1-induced EMT (tEMT) on micro-structured polydimethylsiloxane (PDMS) substrates with variations in stiffness and topographic patterning. *Cell Commun. Adhes.* **2013**, *20*, 115–126.
22. Curtis ASG, Clark. The effects of topographic and mechanical properties of materials on cell behavior. *Crit. Rev. Biocompat.* **1990**, *5*, 343–362.
23. Harrison RG. On the stereotropism of embryonic cells. *Science* **1911**, *34*, 279–281.
24. Tao J, Dong L, Wu Y, Liu X, Xie J, Wu H, et al. Fabrication of room temperature self-healing, robust superhydrophobic coatings via spraying dual cross-linking supramolecular silicone polymer/SiO_2 composite. *Compos. Part B Eng.* **2024**, *273*, 111245.
25. Jiang X, Takayama S, Qian X, Ostuni E, Wu H, Bowden N, et al. Controlling mammalian cell spreading and cytoskeletal arrangement with conveniently fabricated continuous wavy features on poly (dimethylsiloxane). *Langmuir* **2002**, *18*, 3273–3280.
26. Qiu W, Wang Q, Li M, Li N, Wang XX, Yu J, et al. 3D hybrid scaffold with aligned nanofiber yarns embedded in injectable hydrogels for monitoring and repairing chronic wounds. *Compos. Part B Eng.* **2022**, *234*, 109688.
27. Mansouri MR, Fuchs PF, Baghani M, Schuecker C. Matrix–fibre interfacial debonding in soft composite materials: Cyclically behavior modeling and microstructural evolution. *Compos. Part B Eng.* **2022**, *237*, 109853.
28. Li C, Fei J, Zhang T, Zhao S, Qi L. Relationship between surface characteristics and properties of fiber-reinforced resin-based composites. *Compos. Part B Eng.* **2023**, *249*, 110422.
29. Dhar Y, Han YY. Current developments in biofilm treatments: Wound and implant infections. *Eng. Regen.* **2020**, *1*, 64–75.
30. Jayakumar R, Prabaharan M, Kumar PS, Nair SV, Tamura HJB. Biomaterials based on chitin and chitosan in wound dressing applications. *Biotechnol. Adv.* **2011**, *29*, 322–337.
31. Wu P, Nelson EA, Reid WH, Ruckley CV, Gaylor JDS. Water vapour transmission rates in burns and chronic leg ulcers: Influence of wound dressings and comparison with in vitro evaluation. *Biomaterials* **1996**, *17*, 1373–1377.
32. Li Y, Wang J, Wang Y, Cui W. Advanced electrospun hydrogel fibres for wound healing. *Compos. Part B Eng.* **2021**, *223*, 109101.
33. Gauglitz GG, Korting HC, Pavicic T, Ruzicka T, Jeschke MG. Hypertrophic scarring and keloids: pathomechanisms and current and emerging treatment strategies. *Mol. Med.* **2011**, *17*, 113–125.
34. Berman B, Perez OA, Konda S, Kohut BE, Viera M. Delgado S, et al. A review of the biological effects, clinical efficacy, and safety of silicone elastomer sheeting for hypertrophic and keloid scar treatment and management. *Dermatol. Surg.* **2007**, *33*, 1291–1303.
35. Tran B, Wu JJ, Ratner D, Han G. Topical scar treatment products for wounds: a systematic review. *Dermatol. Surg.* **2020**, *46*, 1564–1571.
36. Güneri A. *Handbook of Composite Fabrication*; iSmithers Rapra Publishing: Shropshire, UK, 2001.
37. Abdul-Bari MM, McQueen RH, Nguyen H, Wismer WV, de la Mata AP, Harynuk JJ. Synthetic clothing and the problem with odour: Comparison of nylon and polyester fabrics. *Cloth. Text. Res. J.* **2018**, *36*, 251–266.
38. Shurbaji S, Anlar GGA, Hussein E, Elzatahry A, Elzatahry C, Yalcin H. Effect of flow-induced shear stress in nanomaterial uptake by cells: Focus on targeted anti-cancer therapy. *Cancers* **2020**, *12*, 1916.
39. Corrales T, Larraza I, Catalina F, Portolés T, Matesanz M, Abrusci C. In vitro biocompatibility and antimicrobial activity of poly (ε-caprolactone)/montmorillonite nanocomposites. *Biomacromolecules* **2012**, *13*, 4247–4256.
40. Wu C, Huang J, Chu B, Deng J, Zhang Z, Tang S, et al. Dynamic and hierarchically structured networks with tissue-like mechanical behavior. *ACS Nano* **2019**, *13*, 10727–10736.
41. Zhang M, Chu L, Chen J, Qi F, Li X, Chen X, et al. Asymmetric wettability fibrous membranes: Preparation and biologic applications. *Compos. Part B Eng.* **2023**, *269*, 111095.
42. Shi S, Wu H, Zhi C, Yang J, Si Y, Ming Y, et al. A skin-like nanostructured membrane for advanced wound dressing. *Compos. Part B Eng.* **2023**, *250*, 110438.
43. Lui KC, Wang X, Kan CW. Tuning the tensile and shear properties of a scar healing composite for mechanotherapy. *J. Compos. Sci.* **2024**, *8*, 22.